Available online at www.sciencedirect.com

ScienceDirect

Procedia CIRP 145 (2026) 85–90

www.elsevier.com/locate/procedia

19th CIRP Conference on Computer-Aided Tolerancing (CAT 2026)

Autonomous Design of Uncertainty-Aware Gripper Finger Using Skin Model Shapes

Dominik Koch[†a,*], Sven Wimmer[†a], Jan Baumgaertner[†a], Martin Benfer[a], Gisela Lanza[a]

[a] *wbk Institute of Production Science, Karlsruhe Institute of Technology (KIT), Kaiserstr. 12, 76131 Karlsruhe, Germany*

* Corresponding author. Tel.: +4915239502626. *E-mail address:* dominik.koch@kit.edu
[†] These authors contributed equally to this work.

Abstract

Robust grasping with parallel gripper fingers is often limited by part-to-part geometric variability and uncertainties in object pose, making conventional gripper finger design time-consuming and sensitive to deviations from the nominal shape. This paper presents an uncertainty-aware workflow for automated synthesis of two-finger grippers that integrates Skin Model Shapes as conservative envelopes of end-of-life object realizations in circular production. Candidate finger configurations are parameterized by finger width and immersion depth and evaluated by an algorithm that accounts not only for contact area but also for the resulting forces, while ensuring that the grasp remains feasible within the gripper's stroke and collision limits. The resulting design is instantiated as a two-part finger set comprising a rigid base finger with an undercut-free, from Skin Model Shape derived contact cavity and a replaceable compliant insert, locally refined on the nominal model. The method is evaluated in an industrial robot cell using repeated grasp-and-lift trials on one nominal part and three deliberately modified variants, applying systematic pose perturbations. Object pose is tracked after gripper closure and after a standardized motion sequence, and performance is benchmarked against a nominal-cut rigid baseline and standard/universal fingers. The results demonstrate manufacturable output generation and reduced post-motion rotational pose drift for the proposed design across the considered variants, while also indicating geometry-dependent failure cases that motivate extensions of the uncertainty bounds and contact-surface synthesis.

© 2026 The Authors. Published by Elsevier B.V.
This is an open access article under the CC BY-NC-ND license (https://creativecommons.org/licenses/by-nc-nd/4.0)
Peer-review under responsibility of the scientific committee of the 19th CIRP Conference on Computer-Aided Tolerancing (CAT 2026)

Keywords: Skin Model Shapes; uncertainty-aware design; gripper finger synthesis; compliant inserts; circular production

1. Introduction

Returned products in circular manufacturing frequently deviate from nominal CAD due to wear, deformation, or damage [1]. In robotic disassembly and remanufacturing, such variability causes uncertain contacts, pose deviations, and unstable grasps. Conventional finger design workflows typically rely on nominal geometry if at all, only compensate via adding generic compliance [2], which can fail for systematic or localized deviations, such as a corner being broken off, or some material buildup during its lifecycle. As a result, finger designs that work on nominal parts may not remain reliable across end-of-life (EOL) variants and placements. We address this gap by using Skin Model Shapes (SMS) to represent structural uncertainty and generate uncertainty-aware designs via an automated finger synthesis pipeline. This paper makes three contributions. First, we propose an SMS-based workflow for uncertainty-aware two-finger design under geometric and pose variability. Second, we introduce a force-aware finger evaluation and sizing approach that explicitly evaluates grasp stability instead of just relying on form closure alone. Third, we show that nominal-rigit cut and standard fingers cause large deviations in the grasped object when geometry and position vary, based on experiments with a sample workpiece under three different structural conditions. In contrast, our method produces much smaller errors.

2. Related work

Robotic handling with parallel grippers typically requires application-specific finger geometries to maintain a stable object pose under static and dynamic loads [3]. In practice, this requirement leads to object-specific fingers that must be manually redesigned, a process that is time-consuming and prone to failure when the manufactured part deviates from its nom-

2212-8271 © 2026 The Authors. Published by Elsevier B.V.
This is an open access article under the CC BY-NC-ND license (https://creativecommons.org/licenses/by-nc-nd/4.0)
Peer-review under responsibility of the scientific committee of the 19th CIRP Conference on Computer-Aided Tolerancing (CAT 2026)
10.1016/j.procir.2026.02.109

inal model. This challenge is especially pronounced in circular manufacturing and remanufacturing, where returned parts vary widely in tolerance, wear, and damage and often cannot be placed in magazines, leading to large pose uncertainties during handling [4, 1]. While [5] surveys automated finger design, we categorize prior work into geometric contact shaping (e.g., nominal-cut/dipping), optimization- and learning-driven synthesis, and uncertainty-tolerant strategies using compliance or conservative envelopes. A common geometric baseline is the ”nominal-cut” or ”dipping” principle, where the nominal object model is incrementally inserted into a rigid finger blank, and the contact shape is generated by Boolean subtraction to obtain a collision-free cavity [2]. Complementary jaw-design work addresses robustness from the gripper side by defining admissible jaw tolerance classes that guarantee alignment and form-closure under jaw shape variations [6] and optimizing parallel-jaw tip surface designs for robust grasping via rapid prototyping and large-scale evaluation [7]. Although these methods enable rapid customization, especially via additive manufacturing, they focus primarily on gripper-side variability and typically assume a nominal object model. As a result, they provide limited robustness to substantial deviations in the object itself. Beyond purely geometric designs, optimization-driven methods automate finger synthesis by searching over finger parameters and contact configurations under physical and manufacturability constraints [8]. Recent work further reduces manual effort by coupling finger synthesis with learning-based generation of object-specific forms [9]. Uncertainty is often addressed via conservative clearances or safety margins (e.g., for collision avoidance/insertion), rather than being modeled explicitly as a set of plausible object geometries and poses that drives contact-shape synthesis. When modeled, variability is frequently reduced to tolerances on a few key dimensions instead of a propagated 3D shape-variability model. To mitigate pose and contact uncertainty, many grippers introduce compliance through soft pads, elastic structures, or underactuated mechanisms, often combined with conservative geometric clearances to prevent collisions and jamming under deviations [2]. While effective, these approaches typically treat uncertainty as global and uniform, rather than accounting for the fact that some regions of an object’s geometry may exhibit substantially larger variability than others. A representative geometry-side strategy in battery manufacturing addresses connector pose uncertainty by removing material to avoid collisions across pose variations [10]. Although this increases the admissible pose range, it does so uniformly and may reduce contact adequacy, thereby compromising grasp feasibility under task-specific requirements. In tolerancing research, geometric variability is modeled explicitly and propagated using Skin Model Shapes (SMS) within the GeoSpelling framework [11]. These SMS can be directly generated from measurements of EOL products, such as an inspection station [12]. For automated finger design, SMS therefore offers a structured means of representing spatially varying 3D shape and pose uncertainty, enabling contact-feasibility assessment without relying on ad hoc margins or purely clearance-based heuristics. Building on this idea, we use an SMS envelope to evaluate contact feasibility and to synthesize an undercut-free cavity suitable for additive

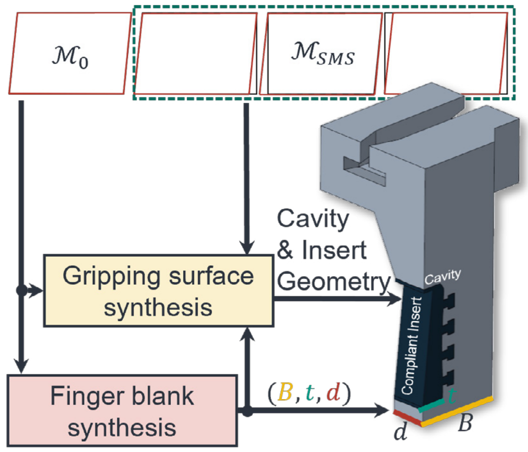

Fig. 1: Overview of the proposed automated finger design workflow. Starting from the nominal object model $\mathcal{M}_0$ and the SMS uncertainty envelope $\mathcal{M}_{\text{SMS}}$, we synthesize a rigid finger blank and the gripping surface, yielding the cavity–insert contact interface parameterized by (B, t, d).

manufacturing. We further combine this cavity with an interchangeable compliant insert to accommodate residual pose and contact uncertainty (see Fig. 1).

3. Uncertainty-aware finger design

This section proposes a four-stage methodology for the automated synthesis of a two-finger gripper set with compliant contact interfaces. Each finger is designed as a two-part assembly comprising a rigid base finger that interfaces with the gripper coupling and a replaceable compliant insert that forms the object-contact surface.

Figure 1 summarizes the pipeline. The remainder of this section is organized as follows: we generate the SMS uncertainty envelope, parameterize the finger and gripper accordingly, design the rigid base finger, and finally derive an undercut-free cavity and matching compliant insert through iterative Boolean operations.

3.1. Skin Model Shape as uncertainty envelope

An SMS is a conservative geometric envelope that represents all admissible surface realizations under expected variability. In our setting, we construct the SMS by combining two sources of uncertainty: object-side geometric variability, represented by a set of measured object variants, and pose variability, represented by bounded rigid-body transformations. In Fig. 1 we consider a trapeziod shaped workpiece with three EOL variants. Overlaying the surface meshes of these four variants yields a model of worst-case scenarios that conservatively bounds the geometric deviations observed in the data. Pose uncertainty is then incorporated by applying bounded rigid-body transformations to this worst-case mesh. The resulting set of transformed surfaces forms the SMS uncertainty envelope (Fig. 2b), providing a conservative approximation of all surfaces that may occur within the assumed geometric and pose bounds. To generate the

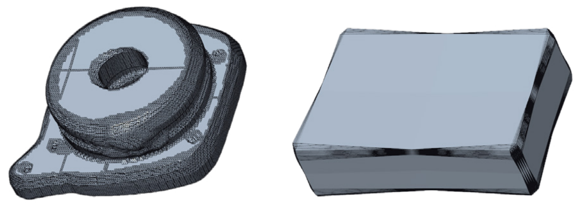

(a) Resulting SMS for a gear from a EOL angle grinder (b) Resulting SMS envelope for the trapezoid

Fig. 2: SMS generation for the reference object: (a) bevel gear of an EOL angle grinder with local deviations(b) resulting conservative SMS envelope by superimposing the mesh with pose variations in y and (a, b, c).

SMS, the worst-case mesh is transformed over the selected pose degrees of freedom within predefined bounds, and the set of transformed instances is aggregated into an envelope (Fig. 2b). Translation along the gripper closing direction is omitted because deviations in this direction are intended to be compensated by the compliant insert during grasping. Translation in z is omitted here because it does not affect the contact cross-section relevant to cavity synthesis in this setup.

3.2. Contact parameterization and design space

In the workflow, the SMS mesh $\mathcal{M}_{\text{SMS}}$ and the nominal object mesh $\mathcal{M}_0$ are the central geometric input for uncertainty-aware design, as it conservatively bounds the admissible object realizations. The design space is defined by two variables: the finger width B and the immersion depth t along the closing direction $\mathbf{d}_c$. We choose (B, t) because B directly sets the lateral extent (and thus the available contact area), while t controls the engagement depth/enclosure along $\mathbf{d}_c$ and thereby the slice evaluated in the layer-wise feasibility check. The feasible ranges for B and t are bounded by the gripper stroke and coupling geometry. The nominal object mesh $\mathcal{M}_0$ is used to shape the insert contact surface to ensure nominal conformity, while a fixed grasp pose defines the grasp frame and the closing direction $\mathbf{d}_c$, which are used throughout the slicing and cavity-generation steps. Moreover, task and interface parameters are provided as design constraints: the required holding force F_H, an estimate of the friction coefficient μ at the insert-object interface, and the allowable contact pressure p_{allow} of the compliant material (as well as gripper-side limits such as stroke and coupling geometry).

3.3. Contact selection and stiffness-based finger dimensioning

Based on the design space (B, t) defined in Sec. 3.2, the workflow instantiates a concrete grasp configuration and derives the main finger dimensions. In this step, compliance is considered only at the level of stiffness-based sizing; the actual cavity and insert geometries are generated in Sec. 3.4. First, the object is placed deterministically in the grasp frame (grasp point at the origin, prescribed grasp orientation), and a safety offset is applied to maintain clearance to the reference plane. Next, it is verified that the object can be positioned collision-free between fully opened fingers, which is a prerequisite for the lateral approach and closing. If feasible, a minimum inter-finger distance is determined to ensure that the rigid finger bodies do not touch until the compliant material is fully compressed, thereby preserving the intended compensation for contour deviations. We evaluate candidate contacts by sweeping the finger width B and immersion depth t on a discrete grid. Larger immersion depths generally increase the available contact area and, consequently, the frictional force capacity, but they also impose tighter geometric constraints on the finger geometry. For each parameter pair (B, t), we analyze the object layer-wise at depth t along the closing direction $\mathbf{d}_c$ and obtain two opposing contact patches, $\Gamma_L(B, t)$ and $\Gamma_R(B, t)$. To remain conservative, we define the effective contact area $A(B, t)$ as the smaller of the two patches. Feasible candidates must transmit the required holding force F_H through Coulomb friction without exceeding the allowable insert pressure p_{allow}, which yields the full minimum-area constraint:

$$A(B, t) = \min(|\Gamma_L(B, t)|, |\Gamma_R(B, t)|) \tag{1}$$

$$A(B, t) \geq A_{\min}, \qquad A_{\min} = \frac{F_H}{2\,\mu\, p_{\text{allow}}}. \tag{2}$$

We further discard candidates that violate gripper constraints (stroke/clearance/collision). Finally, a geometric moment-equilibrium check excludes asymmetric opposing contacts in a symmetric pinch grasp; in practice, this is implemented as an alignment test of the two contact placements (geometry-based, without explicit contact mechanics). Among all feasible candidates, we select (B^*, t^*) by minimizing the compactness objective

$$\min f(B, t) = B^2 + t^2, \tag{3}$$

which discourages unnecessarily wide fingers and excessive enclosure. Ties are resolved by maximizing $A(B, t)$. To localize compliance at the contact interface, we impose a stiffness-ratio constraint between the rigid finger and the compliant insert. We dimension the rigid finger such that, under the same load, its elastic deflection remains smaller than that of the insert. Rigid finger and compliant insert are approximated as linear springs in series, $k_{\text{tot}}^{-1} = k_{\text{finger}}^{-1} + k_{\text{insert}}^{-1}$, with $k_{\text{insert}} = E_{\text{insert}}A/b$ and a cantilever approximation $k_{\text{finger}} = 3E_{\text{finger}}I/L^3$, where $I = BH^3/12$. Enforcing a stiffness hierarchy $k_{\text{finger}} = \alpha\, k_{\text{insert}}$ (with $\alpha = 2$ in this work) yields the minimum required finger thickness:

$$H = L\left(\frac{\alpha \cdot 12 \cdot k_{\text{insert}}}{3E_{\text{finger}}B^*}\right)^{\frac{1}{3}}, \qquad k_{\text{insert}} = \frac{E_{\text{insert}}A^*}{b}. \tag{4}$$

The finger stiffness was experimentally tested for different infill geometries by applying a known force to the infill and measur-

(a) Experiment Setup

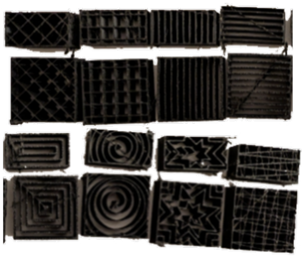

(b) Different tested infills

Fig. 3: Setup for experimental finger stiffness measurement (a) and overview of the tested infill geometries (b). A defined force was applied and the resulting deformation recorded; the gyroid infill was selected due to its most isotropic and linear behavior.

ing the resulting deformation curves. The experiment is shown in Fig. 3 and was performed using Grid (45°), Lines (0,90°), Concentric (45°), Archimedean Chords (45°), Octagram Spirals (45°) and Gyroid infill. In the end Gyroid infill was chosen as it has the most isotropic and linear behavior. The total finger thickness is obtained by adding the selected immersion depth t^* and the insert thickness b to the minimum rigid-finger thickness given by (4). The finger length is chosen to fully cover the engaged object region in the closing direction, plus the predefined safety offset.

3.4. Geometry synthesis of rigid fingers and compliant inserts

The final step realizes the selected parameters (B^*, t^*) as a two-part finger assembly (Fig. 1): a rigid base finger with a contact cavity and a matching compliant insert forming the object-contact interface. The contact surface of the compliant insert follows the classic dipping approach where the fingers are slowly pushed into the nominal object geometry $\mathcal{M}_0$ along the closing direction $\mathbf{d}_c$ until the target immersion depth t^* is reached. Using boolean subtraction, the final contact surface is determined. To account for structural deviations, this process is repeated for the SMS envelope $\mathcal{M}_{\text{SMS}}$. This returns a second contact surface that bounds the compliant insert and forms the cavity where it is inserted. Finally, form-fit assembly features (e.g., grooves/keys) are integrated into the finger and insert to ensure repeatable mounting and prevent relative motion during operation. All components are exported as separate, watertight STL meshes for fabrication by fused deposition modeling. A minor post-processing step removes construction-related protrusions on the insert that would otherwise impair its compensation behavior.

As a qualitative illustration of the cavity–insert concept on a more complex EOL geometry, Fig. 4 shows the resulting finger design for a EOL bevel gear based on the SMS in Fig. 2a. The local deviation induces a protrusion in the compliant insert and a corresponding adaptation of the rigid cavity geometry. This example is included for illustration; the quantitative evaluation in Sec. 5 is reported for the trapezoid variants.

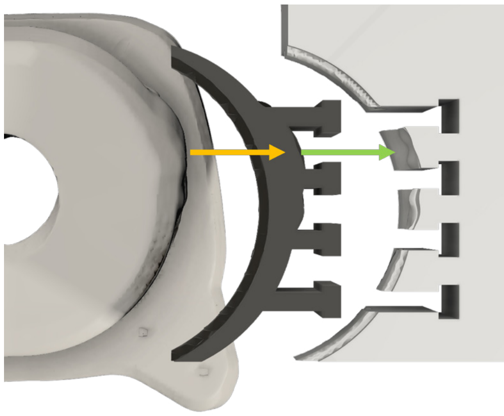

Fig. 4: Qualitative illustration on an EOL bevel gear: a local geometric deviation induces a protrusion in the compliant insert; the rigid finger cavity is adapted accordingly to preserve contact feasibility. The quantitative evaluation in Sec. 5 is conducted on the trapezoid object variants.

4. Experimental setup

This section describes the experimental setup used to evaluate robustness of the proposed uncertainty-aware finger design (Sec. 3) under controlled geometric and pose variability. We quantify performance by measuring the object pose after grasp closure and after a standardized motion sequence, allowing us to assess whether a grasp remains within predefined pose tolerances. We then introduce the robot cell and pose measurement implementation, the test objects and variability model, the trial procedure and perturbation plan, and the baselines.

4.1. Hardware and pose measurement

All grasping experiments are executed with an electric parallel gripper (Schunk EGU-70-PN-N-B) mounted on a 6-axis industrial robot (Comau NJ290-3.0), based on the setup described in [13]. For the latter, the robot executes repeatable grasp trials while systematic pose perturbations are applied. Object pose is measured optically using an overhead camera and a custom evaluation script based on a 2×3 ArUco marker board attached to each object, as shown in Fig. 5. To mitigate imaging distortions, the camera system was calibrated once after the experimental setup using a calibration target.

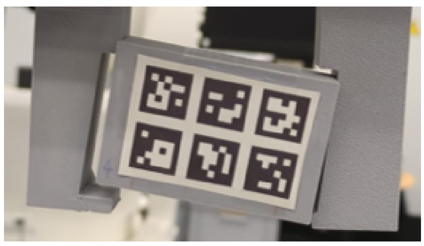

Fig. 5: ArUco-based pose tracking during grasp experiments: the object is equipped with a 2×3 marker board to estimate its pose. In this case the state of the art gripper exhibits large tilting with EOL Variant 2 showing that only considering nominal geometries is not enough.

(a) Proposed Design

(b) Nominal-cut state of the art fingers

(c) Standard/universal fingers

Fig. 6: Finger designs (a-c) used for experimental comparison

4.2. Test objects and variability

In practice, EOL parts exhibit complex, component-specific wear, chipping, and deformation, which makes it difficult to isolate individual uncertainty sources in a controlled and repeatable experiment [1, 4]. To enable systematic evaluation of uncertainty-aware finger synthesis, we therefore use simplified replacement geometries. This approach emulates EOL-like deviations while ensuring reproducibility. Figure 1 illustrates the resulting nominal and EOL object variants. The introduced variants intentionally amplify local deviations to produce grasp-relevant shape differences and to serve as a controlled stress test under pronounced geometric variability. For this study, we summarize geometric variability using a conservative envelope obtained by overlaying all variants.

To incorporate pose uncertainty, the worst-case model is additionally varied in pose. Specifically, we add translational deviations of ±1 mm in y and rotational deviations of ±2° about a, b, c based on the pose estimation system used in [13].

4.3. Design of experiments and trial procedure

To probe the uncertainty represented by the SMS in a systematic and controlled manner, we employ a two-level perturbation plan with fixed bounds ($y = \pm 1$ mm and $a, b, c = \pm 2°$), yielding a full-factorial design with $2^4 = 16$ pose combinations per object and finger type. Within each series, the object geometry is fixed while the perturbation varies between trials. Each experiment follows a fixed sequence adapted from [5]: the object is placed at a predefined reference pose, the robot approaches with the commanded perturbation and closes the gripper to its mechanical end stop, and the first pose is recorded (measurement 1). The robot then lifts the object and executes a dynamic manipulation sequence (300 mm linear motion at 7000 mm/min followed by a return motion with high acceleration and braking to induce inertial loads). Before placing the object on the platform, it is held 10 mm above the platform, and a second pose is recorded (measurement 2). Finally, the object is returned to the start position and, if necessary, small manual corrections are applied to re-establish the reference pose for the next run. To demonstrate the need for explicit treatment of geometric and pose uncertainty, we compare the automatically generated finger set against two baseline designs under identical conditions: state-of-the-art fingers that "dip" into the nominal object geometry during rigid finger design, and standard (universal) fingers (All shown in Fig. 6).

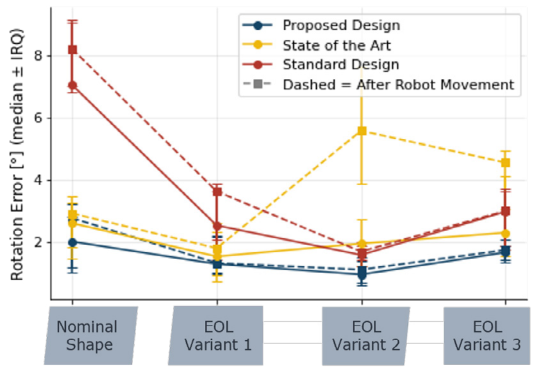

Fig. 7: Rotational pose deviation for the nominal object and three EOL variants for the proposed finger design and two baselines. Solid curves report the error after grasp closure, while dashed curves report the error after the subsequent robot motion sequence. Error bars indicate trial-to-trial variation.

5. Results

5.1. Functional validation: manufacturable geometry export

The functional validation aims to ensure the successful completion of the pipeline and the generation of additively manufacturable output meshes. For the reference geometry (Fig. 1), the method produced complete finger sets (left/right rigid fingers and left/right compliant inserts) in STL format. The exported meshes are watertight (no holes) and show consistent normals, enabling direct processing for additive manufacturing.

5.2. Comparison of grasp performance across finger concepts

Fig. 7 summarizes grasp performance in terms of rotational pose deviation, quantified as the rotation error measured with the ArUco-based pose tracking. For each object variant and finger concept, solid markers report the error at measurement 1, whereas dashed markers report the error at measurement 2. Accordingly, the vertical axis indicates how far the grasped object rotates away from the commanded reference pose at these two time points. Error bars show the dispersion across the full-factorial perturbation combinations (median ± Interquartile Range (IQR)). On the nominal geometry, the proposed design yields the smallest median rotation error at both measurements, while the state-of-the-art fingers achieve comparably low errors after closure but show a larger spread. In contrast, the standard fingers show much larger rotation errors even on the nominal part, and these errors grow after the motion sequence. This is likely because the flat fingers do not adequately support the trapezoidal shape, causing the object to tilt during handling. Across the EOL variants, the proposed design maintains consistently low rotation errors and shows only a small change from measurement 1 to measurement 2, indicating strong pose retention during handling. Performance with the state-of-the-art fingers depends strongly on the variant. While rotation errors remain moderate after closure, they increase markedly after the motion sequence for EOL variants 2 and 3, indicating reduced contact robustness under pronounced geometric deviations. An example is shown in Fig. 5. The standard/universal fingers show intermediate performance on the EOL variants, with larger errors and/or dispersion than the proposed design. Overall, rotation errors tend to increase from measurement 1 to measurement 2, which is expected under inertial excitation where micro-slip, elastic settling of compliant materials, and contact reconfiguration can shift the object to a new equilibrium. The reduced post-motion increase observed for the proposed design suggests that the SMS-derived tolerance-admitting cavity, together with the compliant insert, helps maintain a more repeatable effective contact under these dynamic effects.

5.3. Discussion

The separation between solid and dashed markers in Fig. 7 reflects the additional rotational pose error (tilt) induced by the motion sequence after grasp closure. Across all variants, the proposed design shows the smallest post-motion increase, indicating improved rotational pose retention under dynamic loading compared to both baselines. For the nominal-cut fingers, rotation errors increase markedly for some modified variants, which is consistent with contact surfaces shaped for a nominal geometry: deviations can change the realized contact and promote contact reconfiguration under load. By contrast, the SMS-derived cavity admits the modeled variability and, together with the compliant insert, reduces sensitivity to such reconfiguration, resulting in more consistent post-motion behavior. The introduced deviations are intentionally amplified to provide a controlled stress test; absolute error levels and failure rates should therefore not be interpreted as representative for a specific EOL population. Remaining variant-dependent degradations suggest that very large deviations may require wider uncertainty bounds and/or enriched contact-surface synthesis. During development, highly complex SMS envelopes were found to challenge mesh boolean operations and could yield non-manifold intermediate geometries.

6. Conclusion and Outlook

This work investigates Skin Model Shapes (SMS) as conservative uncertainty envelopes for automated two-finger finger design. In experiments with deliberately amplified geometric variants and systematic pose perturbations, the proposed approach consistently showed a smaller post-motion increase in rotational pose error than the baselines, indicating improved pose retention under dynamic loading within the modeled uncertainty. Methodologically, the results support using explicitly represented variability as an input to contact-feasibility assessment and manufacturable cavity–insert synthesis, reducing the need for manual CAD iteration while remaining compatible with additive manufacturing. This is relevant for circular-production settings, where returned parts may exhibit wear/damage and grasp poses are derived from inspection data with limited accuracy. Future work will extend the evaluation to additional industrial parts and deviation patterns to assess generalizability, refine the uncertainty representation and its parameterization based on application data, and improve the robustness of mesh-based geometry processing for complex SMS envelopes. In addition, the workflow will be integrated into a measurement-to-grasp pipeline by coupling inspection outputs with finger synthesis and deployment on the test station.

Acknowledgements

Funded by the Deutsche Forschungsgemeinschaft (DFG, German Research Foundation) - SFB 1574 - Project number 471687386

References

[1] J.-P. Kaiser, D. Koch, F. Stamer, J. Peeters, and G. Lanza. Semantic 3D product modelling for automated inspection in remanufacturing processes. *Journal of Remanufacturing*, 16:Article 1, 2026. doi: 10.1007/s13243-025-00157-8.

[2] A. Schroeffer, C. Rehekampff, and T. C. Lueth. An automated design approach for task-specific two finger grippers for industrial applications. In *2019 IEEE International Conference on Robotics and Biomimetics (ROBIO)*, pages 184–189, 2019. doi: 10.1109/ROBIO49542.2019.8961500.

[3] S. Hesse. *Greifertechnik*. Carl Hanser Verlag, Munich, 2011. ISBN 978-3-446-42422-7.

[4] Gisela Lanza, Tamim Asfour, Jürgen Beyerer, Barbara Deml, Jürgen Fleischer, Michael Heizmann, Kai Furmans, Constantin Hofmann, Alexander Cebulla, Christian Dreher, Jan-Philipp Kaiser, Jan-Felix Klein, Fabian Leven, Simon Mangold, Norbert Mitschke, Nicole Stricker, Julius Pfrommer, Chengzhi Wu, Marco Wurster, and Manuel Zaremski. Agiles Produktionssystem mittels lernender Roboter bei ungewissen Produktzuständen am Beispiel der Anlasser-Demontage. *Automatisierungstechnik*, 70(6):504–516, 2022. doi: 10.1515/auto-2021-0158.

[5] M. Honarpardaz, M. Tarkian, J. Ölvander, and X. Feng. Finger design automation for industrial robot grippers: A review. *Robotics and Autonomous Systems*, 87:104–119, 2017. doi: 10.1016/j.robot.2016.10.003.

[6] T. Zhang, L. Cheung, and K. Goldberg. Shape tolerance for robot gripper jaws. In *Proceedings of the 2001 IEEE/RSJ International Conference on Intelligent Robots and Systems (IROS)*, pages 1782–1787, 2001. doi: 10.1109/IROS.2001.977236.

[7] M. Guo et al. Design of parallel-jaw gripper tip surfaces for robust grasping. In *2017 IEEE International Conference on Robotics and Automation (ICRA)*, pages 2831–2838, 2017. doi: 10.1109/ICRA.2017.7989330.

[8] Mohammadali Honarpardaz, Johan Ölvander, and Mehdi Tarkian. Fast finger design automation for industrial robots. *Robotics and Autonomous Systems*, 113:120–131, 2019. doi: 10.1016/j.robot.2018.12.011.

[9] H. Ha, S. Agrawal, and S. Song. Fit2Form: 3D generative model for robot gripper form design. In *Conference on Robotic Learning (CoRL)*, 2020.

[10] D. Gebauer, P. Geng, A. Hartmann, et al. Uncertainty-integrating, automated design of gripper jaws for robust grasping of electrical connectors. *Production Engineering: Research and Development*, 19:15–27, 2025. doi: 10.1007/s11740-024-01287-x.

[11] B. Schleich, N. Anwer, L. Mathieu, and S. Wartzack. Skin Model Shapes: A new paradigm shift for geometric variations modelling in mechanical engineering. *Computer-Aided Design*, 50:1–15, 2014. doi: 10.1016/j.cad.2014.01.001.

[12] D. Koch, J.-P. Kaiser, F. Stamer, R. Stark, and G. Lanza. Enhancing visual inspection in remanufacturing: A reinforcement learning approach with integrated robot simulation. *Procedia CIRP*, 134:939–944, 2025. doi: 10.1016/j.procir.2025.02.228.

[13] J. Baumgärtner, M. Hansjosten, D. Hald, A. Hauptmannl, A. Puchta, and J. Fleischer. From CAD to POMDP: Probabilistic planning for robotic disassembly of end-of-life products. arXiv preprint arXiv:2511.23407, 2025.